# Standard Model processes at the 100 TeV FCC

*M.L. Mangano[a1], G.Zanderighi[a1] (editors), et al[a2],*

[a1] CERN, PH-TH, CH-1211 Geneva, Switzerland.
[a2] Others

# Contents

---

[1]Editors: M.L.Mangano, G.Zanderighi

[2]Editor: tbd

[3]Editor: J. Rojo; contributors: Han, Tweedie, ....

[4]Editors: D.D'Enterria, P.Skands

[5]Editor: tbd

[6]Editors: tbd; contributors: alpgen, sherpa, aMC@NLO, ....

[7]Editors: tbd; contributors: alpgen, blackhat, sherpa, aMC@NLO, Robens, Campbell,

[8]Contributors: Garzelli/Moch, Cacciari/Nason?

[9]Editor: tbd; contributors: cacciari, nason, czakon, mitov, Re, Caola, Schulze, Rontsch, Campbell, J-A Aguilar-Saavedra, mangano, Gosam, etc

**Abstract**

This report summarises the properties of Standard Model processes at the 100 TeV $pp$ collider. We document the production rates and typical distributions for a number of benchmark Standard Model processes, and discuss new dynamical phenomena arising at the highest energies available at this collider. We discuss the intrinsic physics interest in the measurement of these Standard Model processes, as well as their role as backgrounds for New Physics searches.

---

[10]Editor: J-A Agular-Saavedra

[11]Editors: tbd; contributors: alpgen, sherpa, aMC@NLO, Maltoni/Oleari/Alioli/Reina

[12]Contributors: aMC@NLO/Sherpa/Torrielli, arXiv:1407.1623

[13]Contributors: Jaeger, ...

[14]Contributors: Jaeger, ...

[15]Editor: A.Larkowski, contributors: Salam, Pierini, Selvaggi, ...

# 1    Introduction: the goals of this Chapter of the FCC-hh physics report[16]

Standard Model particles play multiple roles in the 100 TeV collider environment. In the context of BSM phenomena, and for most scenarios, new BSM particles eventually decay to the lighter SM states, which therefore provide the signatures for their production. BSM interactions, furthermore, can influence the production properties of SM particles, and the observation of SM final states can probe the existence of an underlying BSM dynamics. SM processes therefore provide both signatures and potential backgrounds for any exploration of BSM phenomena. SM backgrounds have an impact on BSM studies in different ways: on one side they dilute, and can hide, potential BSM signals; on the other, SM processes influence the trigger strategies, since they determine the irreducible contributions to trigger rates and may affect the ability to record data samples of interest to the BSM searches.

The observation of SM processes has also an interest per se. The huge rates available at 100 TeV allow, in principle, to push to new limits the exploration of rare phenomena (e.g. rare decays of top quarks or Higgs bosons), the precision in the determination of SM parameters, and the test of possible deviations from SM dynamics. The extremely high energy kinematical configurations probe the shortest distances, and provide an independent sensitivity to such deviations.

Finally, SM processes provide a necessary reference to benchmark the performance of the detectors, whether in the context of SM measurements, or in the context of background mitigation for the BSM searches.

In this Chapter we review the key properties of SM processes at 100 TeV, having in mind the above considerations. This will serve as a reference for future studies, and to stimulate new ideas on how to best exploit the immense potential of this collider. We shall focus on the production of key SM objects, such as jets, heavy quarks, gauge bosons and the Higgs boson. We shall not address issues like the current or expected precision relative to given processes. On one side, and with some well understood exceptions notwithstanding, leading-order calculations are typically sufficient to give a reliable estimate of the production rates, and assess possible implications for trigger rates, background contributions, and detector spefications. On the other, any statement about the precision of theoretical calculations today will be totally obsolete by the time this collider will operate, and assumptions about the accuracy reach cannot but be overly conservative.

---

[16]Editors: M.L.Mangano, G.Zanderighi

## 2 Technical preliminaries[17]

In most chapters, start from basic plots of rates versus $p_t$, $\eta$. When relevant, give tables with cross-sections versus jet-multiplicities.

### 2.1 Calculational setup

### 2.2 Codes and calculations used

### 2.3 Monte Carlo issues, tools

---

[17]Editor: tbd

# 3 Parton distribution functions[18]

## 3.1 Introduction

PDF evolution to 100 TeV. Range, uncertainties, etc.etc.

## 3.2 Heavy Quark Partons

At 100 TeV, particles with masses around the electroweak scale appear as light as the bottom quark at the Tevatron collision energy of $\sqrt{S} = 2\,\text{TeV}$. When a very heavy scale is involved in the process, the gluon splitting into a top-antitop pair may present a large logarithmic enhancement. For $Q \sim 10\,\text{TeV}$, for instance, $\alpha_s(Q)\log(Q^2/m_t^2) \sim 0.6$, which makes a perturbative expansion of the hard process questionable. Defining a parton distribution function (PDF) for the top-quark inside the proton allows us to resum large collinear logarithms $\alpha_s^n(Q)\log^n(Q^2/m_t^2)$ to all orders $n$ in perturbation theory. Initial heavy quarks have been studied in detail in the context of bottom-initiated processes [1, 2], and the main concepts can be adopted for the top-quark. The NNPDF collaboration has released a top-quark PDF as part of their NNPDF2.3 set [3], which facilitates the implementation.
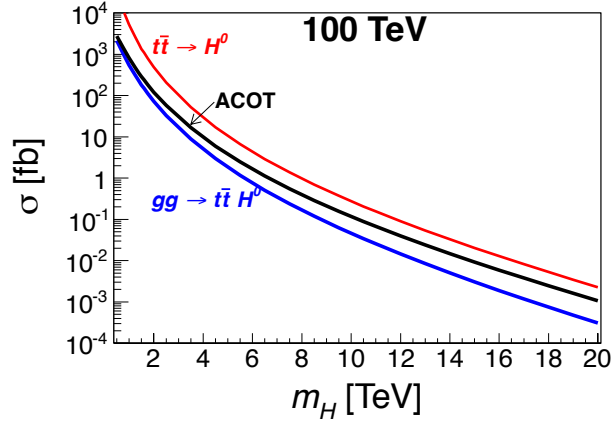


**Fig. 1:** Inclusive cross section for $H^0$ production with Yukawa coupling $y = 1$ at 100 TeV versus its mass $m_{H^0}$, in the 5-flavor scheme (bottom blue), the 6-flavor scheme (upper red), and the ACOT scheme (middle black).

Figure 1 shows a comparison of calculations in the 5-flavor, massless 6-flavor, and ACOT schemes [4, 5] for the inclusive production of a hypothetic heavy scalar ($H^0$) at a 100 TeV pp collider [6]. The ACOT scheme shows the desired behavior of interpolating between the region near the top threshold and the very high energy limit. We point out that the simplest LO 6-flavor calculation is unreliable for masses below 10 TeV, indicating that the minimum scale above which a parton interpretation for the top quark becomes justified is much larger than the top mass itself.

## 3.3 EW bosons as partons

The justification to consider, at very high energy, EW bosons as initial-state partons, is discussed in more detail in Section 7.5, where the relevant technical issues are addressed.

Fig 2 summarizes the parton luminosities when electroweak bosons are included in the PDFs. One immediate observation from comparing the $W_T\gamma$ and $W_TW_T$ luminosities is that transverse weak bosons begin to appear on the same footing as photons, as might have been anticipated. Ultimately, they must be folded into the full DGLAP evolution, though at 100 TeV energies the running effects are not yet sizable.

---

[18]Editor: J. Rojo; contributors: Han, Tweedie, ....
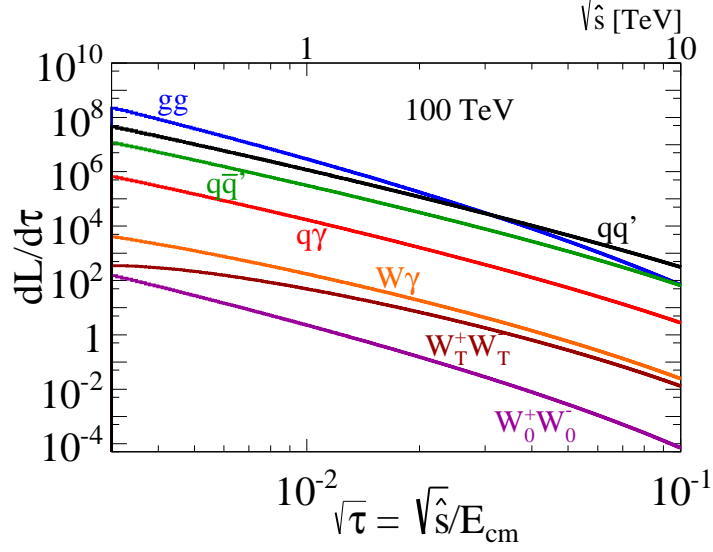
**Fig. 2:** Partonic luminosities at 100 TeV, illustrating the relative contributions from weak bosons when treated as partons in the PDFs [18].

The longitudinal bosons are sourced from the quarks as described above at $p_T \sim m_W$, with individual splitting rates $O(3\text{–}10)$ times smaller than their transverse counterparts at multi-TeV energies. This leads to $O(10\text{–}100)$ times smaller luminosities. For VBF process initiated by the longitudinal bosons, the PDF approach effectively integrates out the usual forward tagging jets, treating them as part of the "beam." This of course becomes a progressively more justifiable approach, as these jets with $p_T \sim m_W$ will appear at extremely high rapidities, and may anyway become a less distinctive feature to discriminate against backgrounds in the presence of copious QCD initial-state radiation at similar $p_T$. From a practical perspective, the ability to treat VBF as a $2 \rightarrow 2$ process rather than $2 \rightarrow 4$ would significantly reduce the computational burden for event simulation. The tagging jets can then be resolved using the usual initial-state radiation machinery, appropriately adapted for this unique electroweak splitting process.

## 4   Global event properties[19]

Discuss Minimum Bias phenomena: multiplicity distributions, $p_T$ spectra, etc. Discuss range of projections from different MC codes, including those used in CR physics. Include as much as possible constraints from LHC13, but the section should not be focused on MC vs data comparisons at the LHC.

Consider separately particle production in the central region and in the forward regions. Expose possible relevance of future measurements by experiments like LHCf.

Cover as well underlying event topics, in particular role of multiparton interactions. For the forward region, present some results relative to minijet production at large rapidity.

---

[19]Editors: D.D'Enterria, P.Skands

# 5  Inclusive vector boson production[20]

The production of $W$ and $Z$ bosons is a valuable probe of both EW and QCD dynamics. The production properties are known today up to next-to-next-to-leading order (NNLO) in QCD, leading to a precision of the order of the percent. A detailed discussion of the implications of this precision, and of the possible measurements possible with $W$ and $Z$ final states at 100 TeV, is outside the scope of this review, also because the LHC has only started exploiting the full potential of what can be done with them. We shall therefore focus here on documenting some basic distributions, to show the extreme kinematical configurations that may be accessed at 100 TeV, and to highlight some of the novel features of EW interactions that will emerge at these energies.
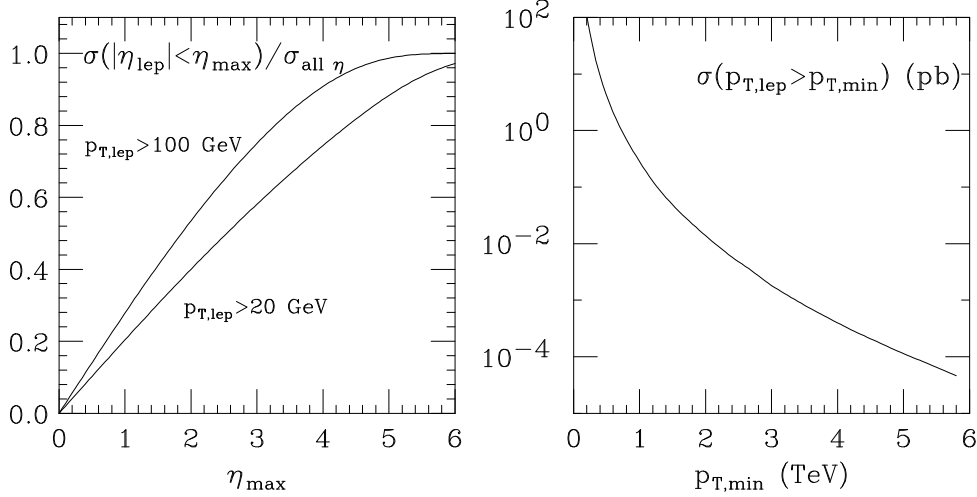


**Fig. 3:** Left: rapidity acceptance for leptons from inclusive $W$ production and decay, for $p_T$ thresholds of 20 and 100 GeV. Right: inclusive lepton $p_T$ spectrum.

The total production rate of $W^{\pm}$ ($Z^0$) bosons at 100 TeV is about 1.3 (0.4) $\mu$b. This corresponds to samples of $O(10^{11})$ leptonic ($e, \mu$) decays per ab$^{-1}$. At 100 TeV, gauge bosons will have a rather broad rapidity distribution and, as shown in the left plot of Fig. 3, more than 50% of the leptons with $p_T > 20$ GeV will be produced at $|\eta| > 2.5$ (w.r.t. $\sim 30\%$ at 14 TeV). Even leptons with $p_T > 100$ GeV will have a large forward rate, with about 40% of them at $|\eta| > 2.5$ ($\sim 10\%$ at 14 TeV). Their $p_T$ spectrum will also extend to large values, as shown in the right plot of Fig. 3. The largest fraction of these high-$p_T$ leptons will arise from $W$'s produced at large $p_T$, in association with jets.

## 5.1  High mass $Z$ and $W$ production

The dilepton mass of DY pairs, at high mass, is shown in Fig. 4.

## 5.2  Diboson production (with discussion of anomalous couplings)

Cover both inclusive and high-mass $V$-pair production. Incorporate here the discussion of EW virtual corrections?

## 5.3  Diphoton production

Cover both issues of relevance to the Higgs backgrounds (e.g. diphoton production in the Higgs-mass region, as a function of $p_T$, up to very large $p_T$), as well as diphoton production at large invariant masses, up to the multi-TeV kinematic limit. Anything known about EW corrections?

---

[20]Editor: tbd
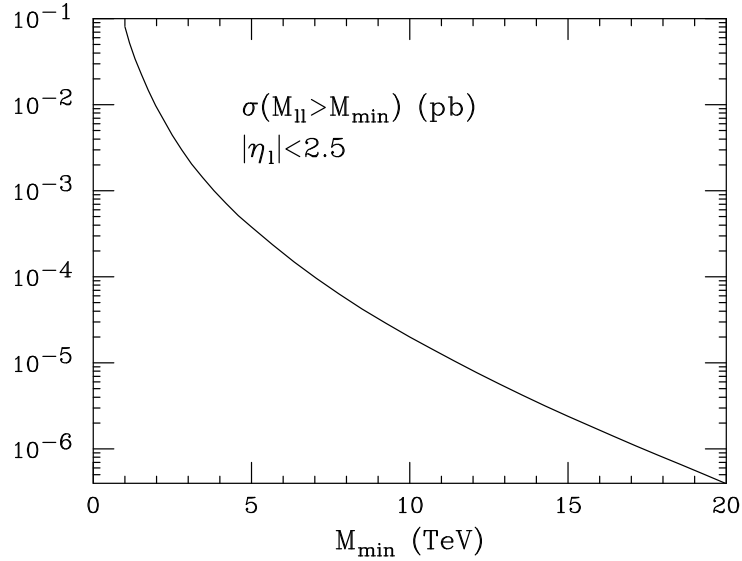
**Fig. 4:** Integrated dilepton invariant mass distribution, for one lepton family, with $|\eta_\ell| < 2.5$.

# 6 Jets[21]

The production of jets is the process that by far dominates, at all distance scales, the final states emerging from hard collisions among the proton consituents.

## 6.1 Inclusive jet and dijet production

Figure 5 shows the integrated rates for the production of events with at least one jet of transverse momentum $p_T$ larger than a given threshold. The distribution refers to jets with pseudorapidity $\eta$ in the range $|\eta| < 2.5$. Figure 6 shows the probability that events with jets above certain $p_T$ threshold be contained inside certain $\eta$ ranges. Notice the huge $\eta$ extension, even for jets with $p_T$ in the TeV range. Assuming integrated luminosities in excess of 1 ab$^{-1}$, the reach in $p_T$ extends well above 20 TeV. Fully containing and accurately measuring these jet energies sets important constraints on the design of calorimeters, e.g. requiring big depth and therefore large transverse size, with a big impact on the overall dimensions and weight of the detectors.
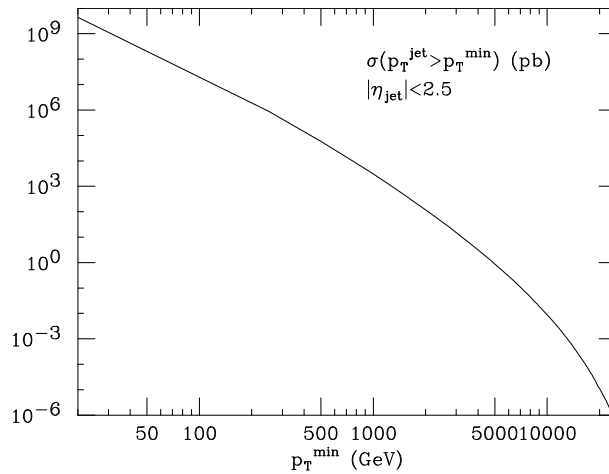


**Fig. 5:** Rates of events with one jet of $|\eta| < 2.5$ and $p_T > p_T^{min}$.

---

[21]Editors: tbd; contributors: alpgen, sherpa, aMC@NLO, ....
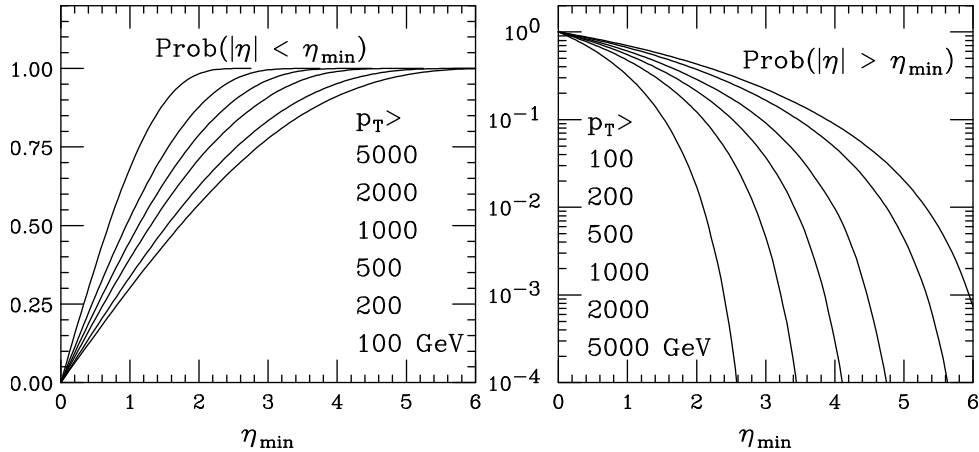
**Fig. 6:** Left: acceptance, for jets above various $p_T$ thresholds, to be contained within $|\eta_j| < \eta_{min}$. Right: probability to be outside the $\eta_{min}$ acceptance.
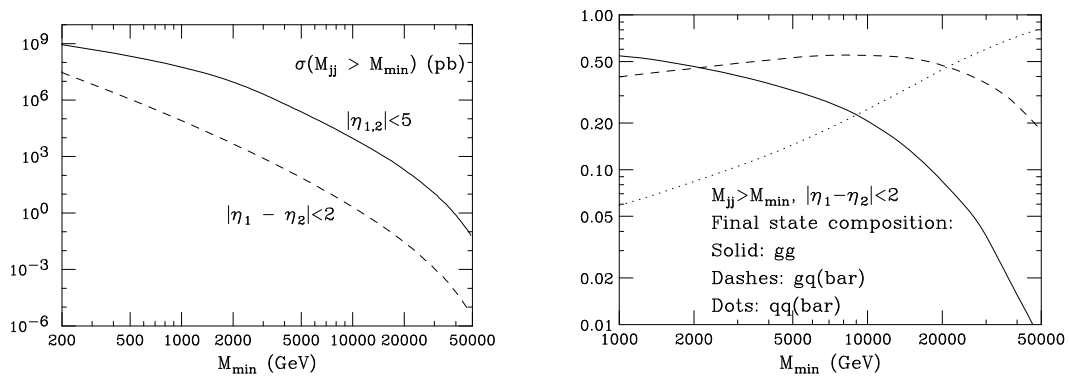


**Fig. 7:** Left: dijet mass spectra, for different $\eta$ constraints. Right: partonic composition of dijet final states, as a function of the dijet mass.

These choices become particularly relevant in the context of searches for high-mass resonances in dijet final states, where the separation from the continuum background of possibly narrow states requires good energy resolution. Figure 7 shows the rates for QCD production of final states with a dijet of invariant mass above a given threshold. We consider two cases: the dijet mass spectrum of all pairs with jets within $|\eta| < 5$, and the spectrum limited to jets produced at large angle in the dijet center of mass ($|\eta_1 - \eta_2| < 2$), a configuration which is more typical of the production and decay of a possible resonance. Notice that, particularly at the largest masses, the former rates are several orders of magnitude larger than the latter ones. This is because one is dominated there by the low-angle scattering. But even for central production we have rates in excess of 1 event/ab$^{-1}$ for masses above 50 TeV. The relative partonic composition of central dijet events, as a function of the dijet mass, is shown in the right plot of Fig. 7. In the region 2 TeV $\lesssim M_{jj} \lesssim$ 20 TeV the final states are dominated by $qg$ pairs. Above 20 TeV, we find mostly $qq$ pairs (the $q\bar{q}$ component is greatly suppressed throughout).

## 6.2 Multi-jet cross sections

Rates, scaling behaviour

## 6.3 Matching at multi-TeV energies

Relevant also for bosons+jets. Make this a separate section, e.g. under "tools" and technical preliminaries ?

11

# 7 Vector bosons and jets[22]

## 7.1 Inclusive rates

## 7.2 Scaling behaviour of $V$ plus multi-jet production

## 7.3 Photons and multi-jet production

## 7.4 Diboson plut jet production

## 7.5 Production of gauge bosons at the highest energies

The left plot in Fig. 8 shows the integrated $p_T$ spectrum of $W$ bosons[23]. With luminosities in excess of $1\ \mathrm{ab}^{-1}$, data will extend well beyond 15 TeV. For processes involving gauge bosons and jets at such large energies, however, a very interesting new phenomenon emerges, namely the growth of the gauge boson emission probability from high-$p_T$ jets. If we ask what is the most likely mechanism to produce gauge bosons in final states with at least one multi-TeV jet, it turns out that this is not the LO QCD process where the gauge boson simply recoils against the jet, but the higher-order process where it is a second jet that absorbs the leading jet recoil, and the gauge boson is radiated off some of the quarks [8]. In other words, the parton-level scattering $qq \rightarrow qqV$ dominates over $qg \rightarrow qV$ (for simplicity, we do not show explicitly the possibly different quark flavour types involved in the processes). The emission probability of gauge bosons in this case is enhanced by large logarithms of $p_{T,jet}/m_V$, and can reach values in the range of 10% and more, as shown in the right plot of Fig. 8. This gives the emission probability for one or more $W$ bosons in events in which there is at least one jet above a given $p_T$ threshold. The kinematical properties of these events are illustrated in Fig. 9, in the case of final states with a jet above 1 TeV, and above 10 TeV, to highlight the kinematical evolution with jet $p_T$. In the case of largest $p_T$, we see the dominance of events in which the two jets balance each other in transverse momentum, while the $W$ carries a very small fraction of the leading jet momentum. One third of the $W$'s are emitted within $\Delta R < 1$ from the subleading jet, with a large tail of emission at larger angles, due in part to $W$ radiation from the initial state.
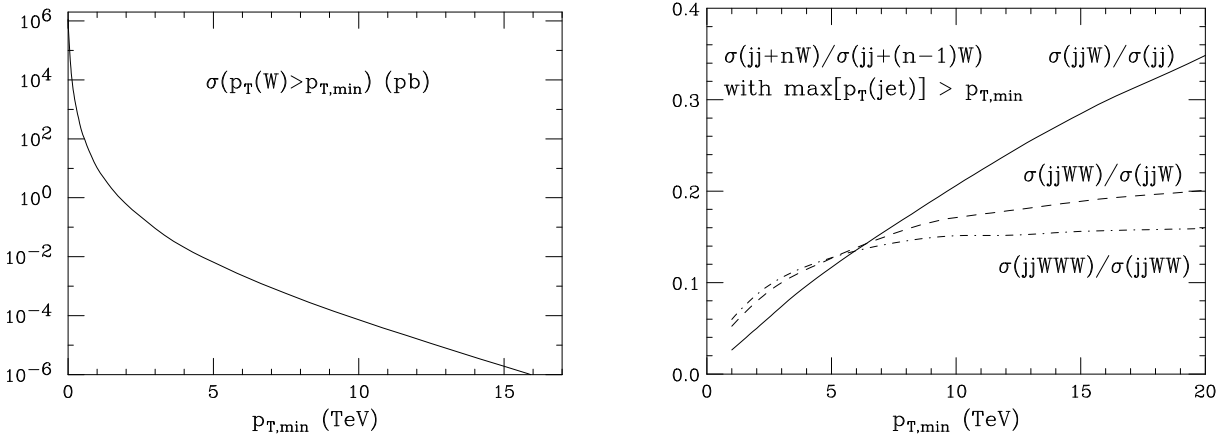


**Fig. 8:** Left: inclusive $p_T$ spectrum of $W$ bosons. Right: emission probability for additional $W$ bosons in dijet events at large $p_T$.

The process considered above is just one manifestation of the general fact that, in hard electroweak interactions at multi-TeV energies, the soft/collinear structure of almost *any* multi-TeV process can become significantly altered, as the logarithmic enhancements familiar from QED and QCD will become active for electroweak emissions (see, e.g., [9–13]). Obtaining correct descriptions of the complete event

---

[22]Editors: tbd; contributors: alpgen, blackhat, sherpa, aMC@NLO, Robens, Campbell,

[23]This calculation only includes the QCD effects. For $p_T$ beyond the TeV scale, the effects of virtual EW corrections are known to lead to important corrections [7].
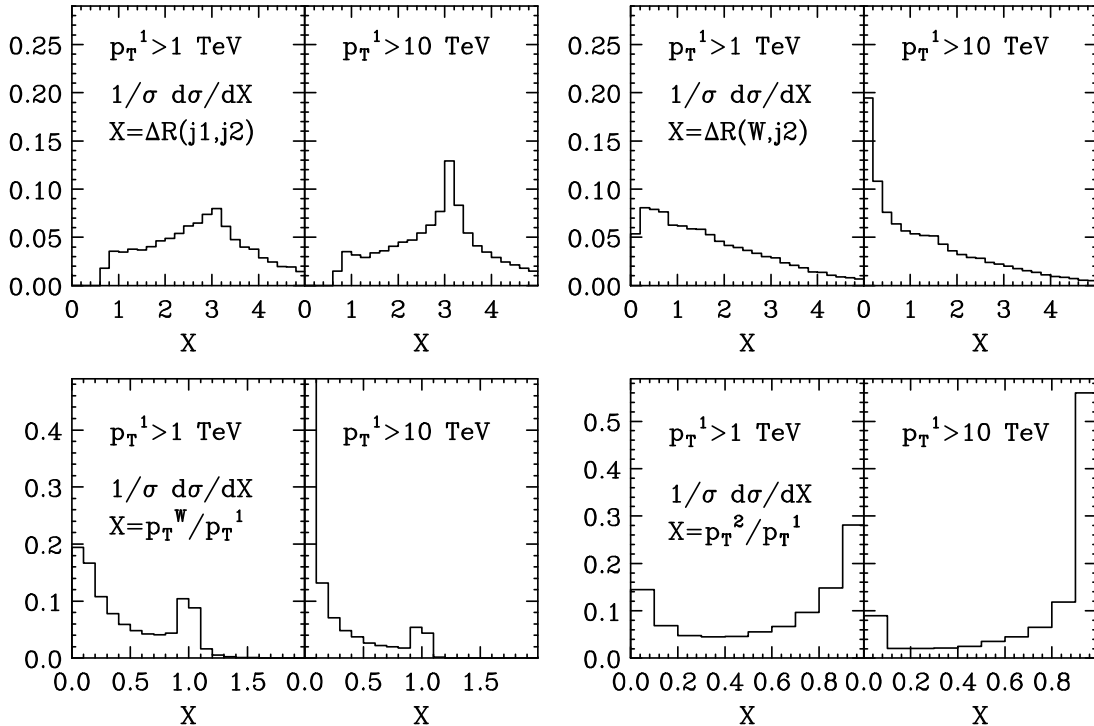
**Fig. 9:** Kinematical correlations in high-$p_T$ jet events with $W$ radiation, for values of the leading jet $p_T > 1$ and 10 TeV.

structure when $\sqrt{\hat{S}} \gg m_W$ can be then greatly facilitated by incorporating factorization and resummation, such as that provided by parton showering and parton distribution functions. In effect, we will begin to see weak bosons (including the Higgs boson) behaving as nearly-massless partons, in stark contrast to the conventional perspective in which they are viewed as "heavy" particles. Jets, whether initiated by QCD processes, electroweak process, or new physics processes, will be found to contain electroweak splittings with probabilities at the $O(10\%)$ level. Similarly, weak bosons can usefully be thought of as collinear components of the protons, at the same level as gluons and photons.

To develop some intuition of the collinear splitting behavior of electroweak "partons," it is useful to first consider a conceptual limit with an unbroken $SU(2) \times U(1)$ gauge symmetry with massless gauge bosons and fermions, supplemented by a massless scalar doublet field $\phi$ without a VEV (the would-be Higgs doublet). In this limit, many processes are direct analogs of those in QED and QCD. Fermions with appropriate quantum numbers may emit (transverse) $SU(2)$ and $U(1)$ gauge bosons with both soft and collinear enhancements. The $SU(2)$ bosons couple to one another via their non-abelian gauge interactions, and undergo soft/collinear splittings of the schematic form $W \to WW$, similar to $g \to gg$. All of the electroweak gauge bosons may also undergo collinear-enhanced splittings into fermion pairs, similar to $g \to q\bar{q}$ or $\gamma \to f\bar{f}$. Beyond these, the major novelty is the introduction of the scalar degrees of freedom. First, the scalars may themselves radiate $SU(2)$ and $U(1)$ gauge bosons, with soft/collinear limits identical to their counterparts with fermionic sources. Second, the electroweak gauge bosons can split into a pair of scalars, again in close analog with splittings to fermion pairs. Third, fermions with appreciable Yukawa couplings to the scalar doublet can emit a scalar and undergo a chirality flip. Finally, the scalars can split into collinear fermion pairs.

In the realistic case of spontaneously-broken symmetry, several important changes take place. Primarily, all of the soft and collinear divergences associated with the above splittings become physically regulated, effectively shutting off at $p_T \lesssim m_W$ (or $m_h$, $m_t$ where appropriate). Roughly speaking, $m_W$ plays a role similar to $\Lambda_{\text{QCD}}$ in the QCD parton shower, albeit with far less ambiguity of the detailed

| Process | $\mathcal{P}(p_T)$ | $\mathcal{P}(1\text{ TeV})$ | $\mathcal{P}(10\text{ TeV})$ |
|---|---|---|---|
| $f \to V_T f$ | $(3 \times 10^{-3}) \left[\log \frac{p_T}{m_{\text{EW}}}\right]^2$ | 1.7% | 7% |
| $f \to V_L f$ | $(2 \times 10^{-3}) \log \frac{p_T}{m_{\text{EW}}}$ | 0.5% | 1% |
| $V_T \to V_T V_T$ | $(0.01) \left[\log \frac{p_T}{m_{\text{EW}}}\right]^2$ | 6% | 22% |
| $V_T \to V_L V_T$ | $(0.01) \log \frac{p_T}{m_{\text{EW}}}$ | 2% | 5% |
| $V_T \to f\bar{f}$ | $(0.02) \log \frac{p_T}{m_{\text{EW}}}$ | 5% | 10% |
| $V_T \to V_L h$ | $(4 \times 10^{-4}) \log \frac{p_T}{m_{\text{EW}}}$ | 0.1% | 0.2% |
| $V_L \to V_T h$ | $(2 \times 10^{-3}) \left[\log \frac{p_T}{m_{\text{EW}}}\right]^2$ | 1% | 4% |

**Table 1:** An illustrative set of approximate total electroweak splitting rates in final-state showers [18].

IR structure since this regulation occurs at weak coupling. Another major difference is the mixing of the scalar doublet's Goldstone degrees of freedom into the $W$ and $Z$ gauge bosons, allowing for the appearance of longitudinal modes. In many cases, the longitudinal gauge bosons behave identically to the original scalars, as dictated by the Goldstone equivalence theorem [14, 15]. For example the splitting $W_T^+ \to W_L^+ Z_L$ is, up to finite mass effects, an exact analog of $W_T^+ \to \phi^+ \text{Im}(\phi^0)$ in the unbroken theory. Similarly for longitudinal gauge boson emissions from heavy fermions, such as the equivalence between $t_L \to Z_L t_R$ and $t_L \to \text{Im}(\phi^0) t_R$.

But important exceptional cases now also occur for emissions near $p_T \sim m_W$. Most well known, even a massless fermion exhibits a kind of soft/collinear-enhanced emission of $W_L$ and $Z_L$ [16, 17]. These emissions have no Goldstone equivalent analog, and are highly power-suppressed for $p_T \gtrsim m_W$. But the overall population of emissions at the boundary between "broken" and "unbroken" behavior nonetheless grows logarithmically with the fermion energy. This is formally subdominant to the double-logarithmic growth of transverse emissions, but remains numerically important at multi-TeV energy scales. Emissions from massless quarks also cause the energetic initial-state protons to act as sources of longitudinal boson beams, allowing for studies of the high-energy interactions of the effective Goldstone bosons through weak boson scattering (discussed further below). Similar types of emissions occur in the splittings of transverse bosons, such as $W_T^+ \to Z_L W_T^+ / Z_T W_L^+$.

Table 1 provides a few estimates for total splitting rates of individual final-state particles, including approximate numerical values for particles produced at $p_T = 1$ TeV and 10 TeV. The $SU(2)$ self-interactions amongst transverse gauge bosons tend to give the largest rates, quickly exceeding 10% as the energy is raised above 1 TeV (these rates are slightly lower than those extracted from Fig. 8, since there an important contribution to $W$ emission came from initial state radiation). This has significant impact on processes with prompt transverse boson production such as $W/Z/\gamma$+jets, and especially on multiboson production including transverse boson scattering. Generally, it is important to appreciate that *any* particle in an event, whether initial-state or final-state, or even itself produced inside of a parton shower, can act as a potential electroweak radiator. Consequently, the total rate for finding one or more electroweak splittings within a given event must be compounded, and can sometimes add up to $O(1)$.

The enhanced $W$ and $Z$ radiation can also have interesting applications in new physics searches. We briefly mention a couple of examples here.

The invisible and semi-invisible decays of a $Z'$ and $W'$ are difficult to probe directly. At large energies, neutrinos can emit $W$ and $Z$ bosons making missing energy visible.[24] The Sudakov enhancement of this process can make the three-body decays of a $W'$ or $Z'$ significant if the leptons are sufficiently boosted, e.g. $Z' \to \nu\bar{\nu}Z$ or $Z' \to \nu l^- W^+$. If a $Z$ boson is radiated, the collinear enhancement results in

---

[24]The importance of heavy $Z'$ three-body decays was first mentioned in Ref. [19] in the context of SSC and later in Ref. [13, 20] in context of a 100 TeV collider.
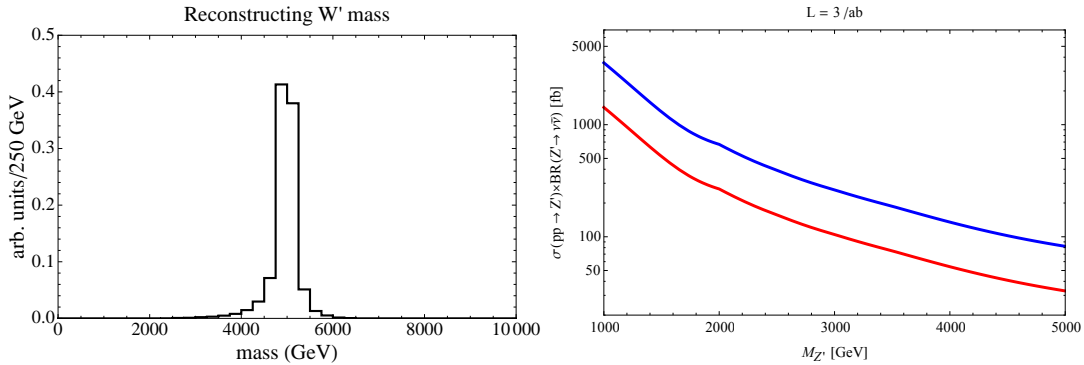
**Fig. 10:** Under the assumption that the neutrino is collinear with the leptonic $Z$, the reconstructed neutrino allows one to guess the real missing energy in an event as well as reconstruct the full mass peak of a $W'$ particle (plot on the LHS). The mass resolution is smeared since the $Z$ is not always collinear with the neutrino, but the peak is very clearly at the $W'$ mass of 5 TeV. On the right hand side, we plot the reach of a 100 TeV collider to a $Z'$ decaying invisibly for a luminosity of 100 fb$^{-1}$ and 3000 fb$^{-1}$. The blue and red lines are the 5 and 2 $\sigma$ results respectively.

a strong tendency for the $Z$ boson to be emitted parallel to the neutrino. Assuming that the $Z$ boson lies completely parallel to the neutrino allows one to reconstruct the neutrino in its entirety. If a $W$ boson is radiated, the neutrino becomes completely visible and tagging its origin as a neutrino is needed. If the $W$ can be reconstructed (most likely in a hadronic decay mode), the small $\Delta R$ distance between it and the lepton allows one to tag the lepton as originating from a neutrino.

These effects at an 100 TeV pp collider have been studied in Ref. [13]. The analysis is at parton level and Madgraph5 [21–23] was used to generate the events. The results are shown in Fig. 10.

Next, we further pursue this approach showing how one can determine quantum numbers of new particles based on total EW gauge bosons emission. Particles which are not charged under $SU(2)_L \times U(1)_Y$ do not radiate $W$ and $Z$ bosons and can thus be distinguished from their charged counterparts.

We illustrate this effect in an example where we assume a "natural SUSY" - like spectrum at the TeV scale, namely a stop as an NLSP decaying into a neutralino LSP. SUSY with light third generation squarks is a well motivated [24, 25] and well studied scenario [26–28]. The left and right handed stops have different couplings to the $Z$. Due to electroweak symmetry breaking, they mix so that the NLSP is an admixture of the two. At large masses, the chirality of the stops can be measured by the additional radiation of a $Z$ or $W$ in the event. The Sudakov enhancement for the radiation of $Z$s and $W$s makes this measurement feasible at a 100 TeV machine. Note however that the radiation of the EW gauge bosons from the stop is only single log enhanced because the collinear singularity in this case is cut off by the mass of the emitting particle (the stop) and effectively does not lead to any enhancement. Meanwhile, both ISR and FSR have a Sudakov double log enhancement. Because both the decay products of the stop and the initial state quarks have the same chirality as the stop, the radiation strength provides a good measure of the chirality of the stop regardless of where the radiation came from.

Fig. 11 demonstrated such a measurement with two benchmark stop masses: $m_{\tilde{t}} = 0.7$ TeV and $m_{\tilde{t}} = 1.5$ TeV, all decaying into a massless bino-like neutralino. Note that the first benchmark point can be easily discovered by the LHC while the second one is inaccessible even for the LHC14. There is a clear difference between $\cos\theta_{\tilde{t}} = 0$ and 1. Thus purely left and purely right handed stops can be distinguished.
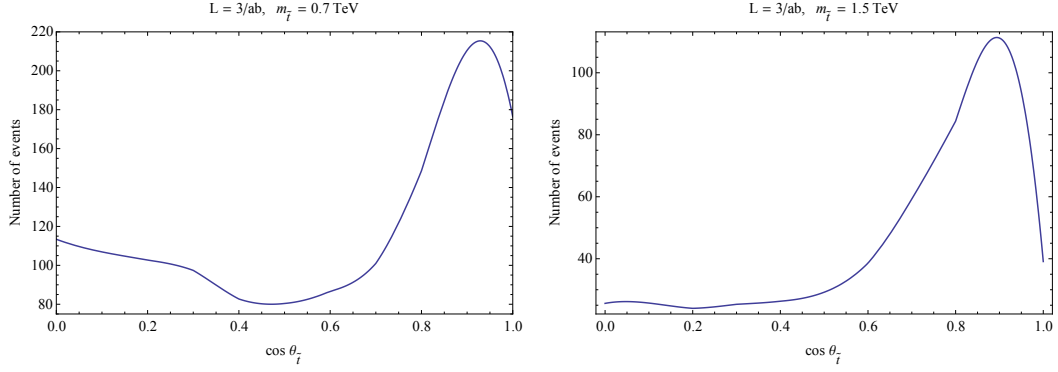
**Fig. 11:** Number of signal events after imposing all selection cuts, detailed in Ref. [13], as a function of $\cos\theta_{\tilde{t}}$ for three mass points. $\cos\theta_{\tilde{t}} = 0$ is a right handed stop.

# 8 Heavy flavour production[25]

## 8.1 Inclusive bottom production

Inclusive production of $b$ hadrons in hadronic collisions offers unlimited opportunities for flavour studies in the $b$ sector, as shown very well by the Tevatron and LHC experiments. The long-term interest in these
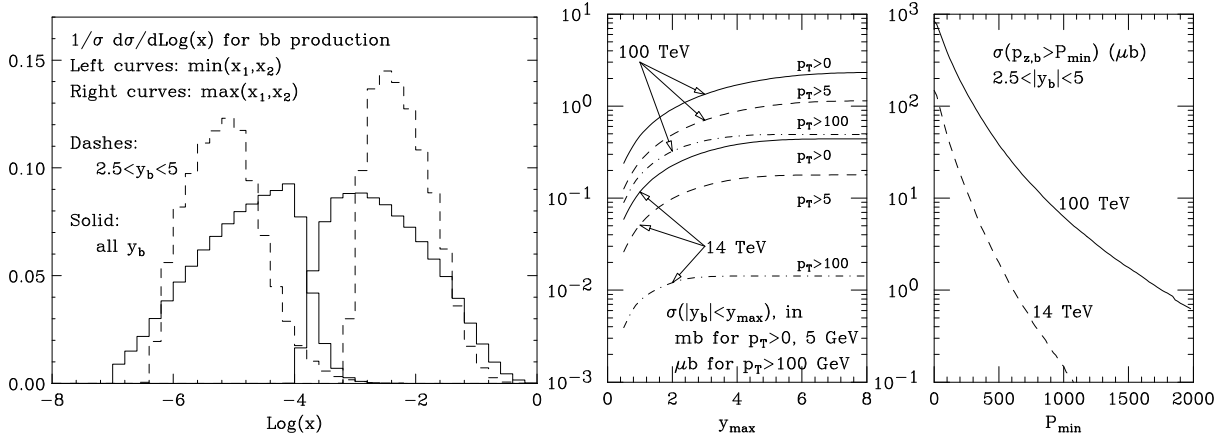


**Fig. 12:** Left: distribution of the smaller and larger values of the initial partons momentum fractions in inclusive $b\bar{b}$ events (solid) and in events with at least one $b$ in the rapidity range $2.5 < |y| < 5$ (dashes). Center: production rates for $b$ quarks as a function of detection acceptance in $y$, for various $p_T$ thresholds (rates in $\mu$b for $p_T > 100$ GeV, in mb otherwise). Right: forward $b$ production rates, as a function of the $b$ longitudinal momentum.

studies will depend on what future LHCb and Belle2 data will tell us, and on the flavour implications of possible LHC discoveries in the high-$Q^2$ region. But it is likely that heavy flavour studies will remain a pillar of the physics programme at 100 TeV. The total $b\bar{b}$ production cross section at 100 TeV is about 2.5mb, and increase of $\sim 5$ relative to the LHC, and it is more than a 1% fraction of the total $pp$ cross section. This rate comes with a large uncertainty, due to the contribution of gluons at very small $x$ values, where the knowledge of PDFs is today extremely poor and mostly dictated, at best, by reasonably guessed extrapolations. The left plot of Fig. 12 shows that, for a detector like LHCb, covering the rapidity region $2.5 < y < 5$, about 50% of the $b$ events would originate from gluons with momentum $x < 10^{-5}$, i.e. in a domain totally unexplored so far! The following two plots of Fig. 12 provide the rapidity distributions for $b$ quarks produced above some thresholds of $p_T$ and, for $b$ quarks produced in the region $2.5 < |y| < 5$, the integrated spectrum in longitudinal momentum $p_z$, comparing results at 14 and 100 TeV. We note that,

---

[25]Contributors: Garzelli/Moch, Cacciari/Nason?

16

while the total production rate grows only by a factor of $\sim 5$ from 14 to 100 TeV, the rate increase can be much greater once kinematic cuts are imposed on the final state. For example, at 100 TeV $b$ quarks are produced in the forward region $2.5 < |y| < 5$ with $p_z > 1$ TeV at the astounding rate of $10\mu$b, 100 times more than at the LHC. To which extent this opens concrete opportunities for new interesting mesurements, to be exploited by the future generation of detectors, remains to be studied.

## 8.2 Inclusive top pair production

Table 2 shows the NLO cross sections for the inclusive production of top quark pairs, and for production in association with one and two gauge bosons. The $\sim 30$ nb inclusive rate is more than 30 times larger than at 14 TeV. For the planned total integrated luminosity, two experiments would produce of the order of $10^{12}$ (anti)top quarks. The possible applications emerging from this huge statistics have yet to be explored in detail. It would be interesting to consider the potential of experiments capable of recording all these events (only a small fraction of top quarks produced at the LHC survives for the analyses). Triggering on one of the tops, would allow for unbiased studies of the properties of the other top and of its decay products: studies of inclusive $W$ decays [29] (which are impossible using the $W$'s produced via the Drell-Yan process), of charm and $\tau$ leptons produced from those $W$ decays, of flavour-tagged $b$'s from the top decay itself [30].
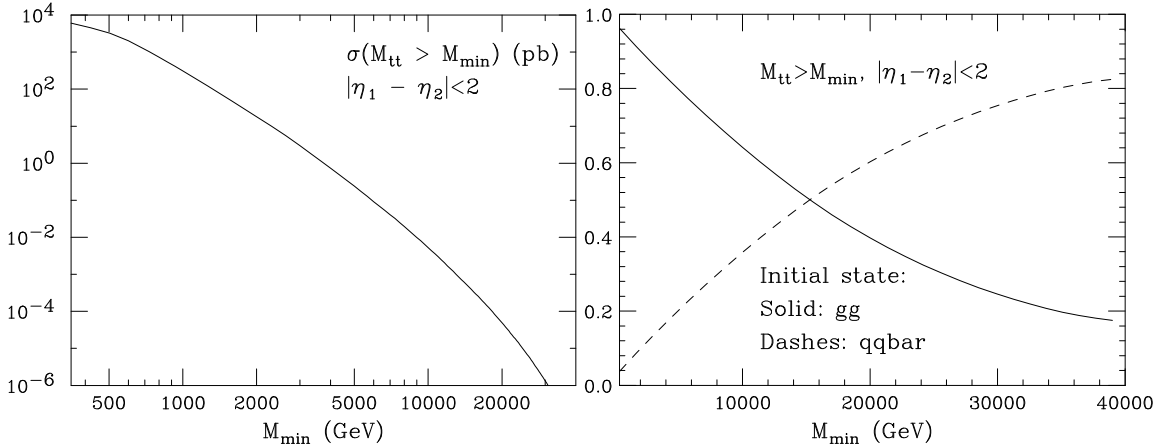


**Fig. 13:** Left: integrated invariant mass distribution for production of central $t\bar{t}$ quark pairs. Right: initial state composition as a function of the $t\bar{t}$ invariant mass.

Comparing the rates for associated production, in Table 2, with those in Table 3 for multiple gauge boson production, and considering that each top quark gives rise to a $W$ through its decay, we remark that top quark processes at 100 TeV will provide the dominant source of final states with multiple $W$ bosons, and thus with multiple leptons. This will have important implications for the search of new physics signals characterized by the presence of many gauge bosons or leptons from the decay of the new heavy particles.

Notice also that $t\bar{t}Z^0$ production is more abundant than $t\bar{t}W^\pm$, contrary to the usual rule that $W$ bosons are produced more frequently than $Z^0$'s in hadronic collisions. This is because the $t\bar{t}Z^0$ process is driven by the $gg$ initial state, which for these values of $\hat{s}/S$ has a much larger luminosity than the $q\bar{q}'$ initial state that produces $t\bar{t}W$. This also implies that studies of top production via initial state light quarks (e.g. in the context of $t$ vs $\bar{t}$ production asymmetries) will benefit from a higher purity of the $q\bar{q}$ initial state w.r.t. $gg$ if one requires the presence of a $W$ boson (see e.g. Ref. [31]).

| | $t\bar{t}$ | $t\bar{t}t\bar{t}$ | $t\bar{t}W^{\pm}$ | $t\bar{t}Z^0$ | $t\bar{t}WW$ | $t\bar{t}W^{\pm}Z$ | $t\bar{t}ZZ$ |
|---|---|---|---|---|---|---|---|
| $\sigma$(pb) | $3.2 \cdot 10^4$ | 4.9 | 16.8 | 56.3 | 1.1 | 0.17 | 0.16 |

**Table 2:** NLO cross sections for associated production of (multiple) top quark pairs and gauge bosons [32, 33].

### 8.3   Bottom and top production at large $Q^2$

Production of bottom and top quarks at large $Q^2$ is characterized by two regimes. On one side we have final states where the heavy quark and antiquark ($Q$ and $\bar{Q}$) give rise to separate jets, with a very large dijet invariant mass $M_{QQ}$. These are the configurations of relevance when, for example, we search for the $Q\bar{Q}$ decay of massive resonances. In the case of top quarks, the left-hand side of Fig. 13 shows the production rate for central $t\bar{t}$ pairs above a given invariant mass threshold. At 100 TeV there will be events well above $M_{tt} > 30$ TeV. The right plot in Fig. 13 furthermore shows that, due to the absence at LO of contributions from $qq$ or $qg$ initial states, $gg$ initial states remain dominant up to very large mass, $M_{tt} \sim 15$ TeV. Well above $M_{QQ} \sim$ TeV, the results for $b\bar{b}$ pair production are similar to those of the top.

The second regime occurs when we request only one jet to be tagged as containing a heavy quark. This could be of interest, for example, in the context of high-$p_T$ studies of single top production. In this regime, configurations in which the heavy quark pair arises from the splitting of a large-$p_T$ gluon are enhanced. The final state will then contain a jet formed by the heavy-quark pair, recoiling against a gluon jet. An example of the role of these processes is shown in Fig. 14, where we compare the $p_T$ spectrum of $b$ jets in events where the $b\bar{b}$ pair is produced back to back (as in the first case we discussed above), and the spectrum of jets containing the $b$ pair (here jets are defined by a cone size $R = 0.4$). The latter is larger by approximately one order of magnitude at the highest $p_T$ values, leading to rates in excess of 1 event/ab$^{-1}$ for $p_T > 15$ TeV. Similar considerations apply to the case of top quark production in this multi-TeV regime, as shown in the right plot of Fig. 14. In this case the rate for $t\bar{t}$ jets is only slightly larger than that for single-top jets, due to the much larger mass of the top quark, which leads to a smaller probability of $g \to t\bar{t}$ splitting.
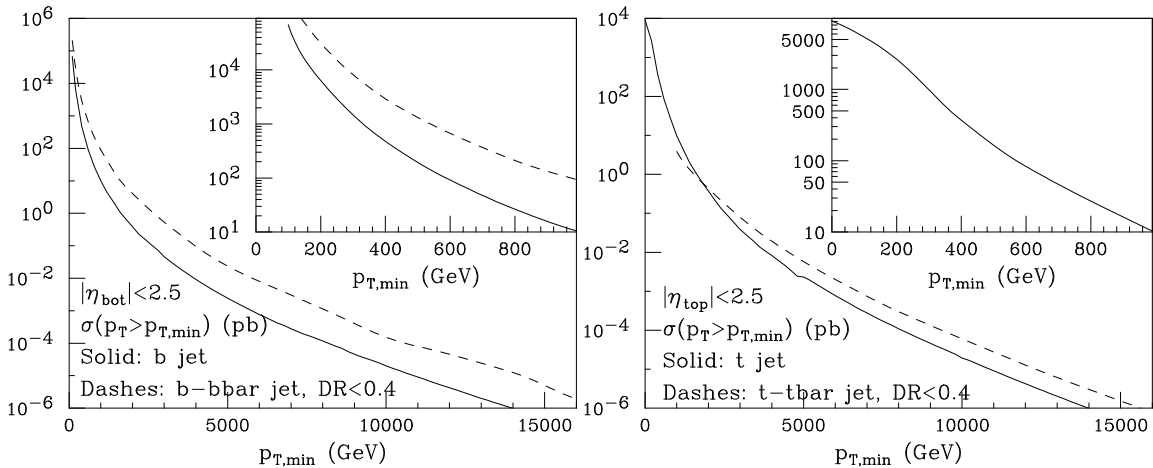


**Fig. 14:** Left: production rates for $b$ jets (solid), and for jets containing a $b\bar{b}$ pair within $\Delta R < 0.4$ (dashes). Right: same, for top-quark jets (top treated as stable).

### 8.4   Single top production

Document production cross sections, both inclusive and in the very high energy limit. For example, the single top $s$-channel production at verylarge invariant mass is shown in Fig. 15.
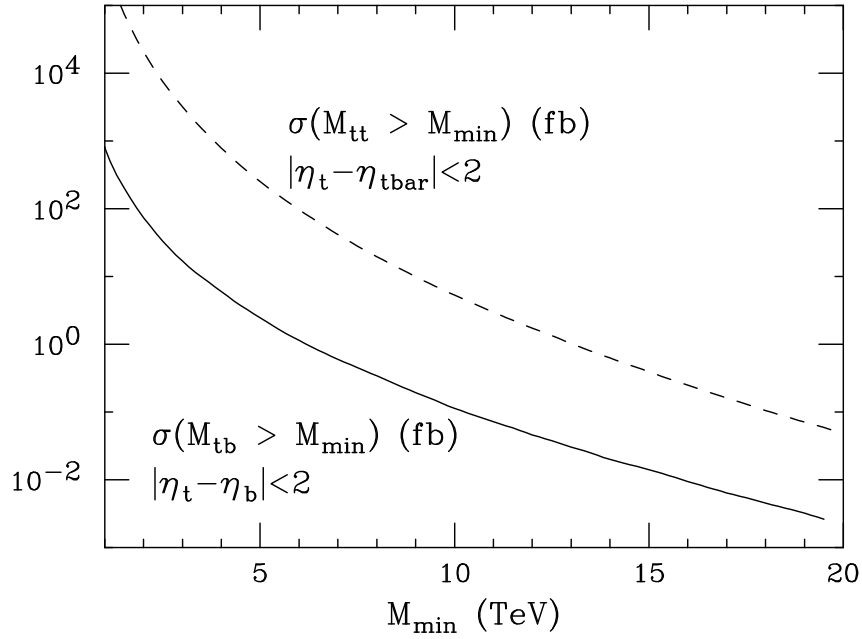
**Fig. 15:** Integrated mass spectrum of central $t\bar{b}$ pairs (and c.c.) in single-top $s$-channel production (solid line). The potential background from inclusive $t\bar{t}$ production is shown by the dashed curve.

# 9    Physics with top quarks[26]

## 9.1    $t\bar{t}Z$ production

Includes anomalous couplings, etc

## 9.2    $t\bar{t}W$ production

## 9.3    $t\bar{t}\gamma$ production

## 9.4    Top properties[27]

Includes rare and forbidden decays, anomalous couplings, FCNC probes through single top production, etc

---

[26]Editor: tbd; contributors: cacciari, nason, czakon, mitov, Re, Caola, Schulze, Rontsch, Campbell, J-A Aguilar-Saavedra, mangano, Gosam, etc

[27]Editor: J-A Agular-Saavedra

## 10 Vector boson and heavy flavours[28]

Cover here $V b\bar{b}$ and $V c\bar{c}$. Leave the production with top quarks to a separate section. Consider, where relevant, both sigle and double $Q$ production. Study in particular the region of $m_{QQ} \sim m_H$, as a background to Higgs production, and consider both the inclusive and the very-high $p_T(QQ)$ region. Considerations relative to the tagging of the $QQ$ jet, using substructure techniques in the very boosted region, could go here or in the dedicated boosted section, to be decided once we have the relevant material.

Is there a potential interest in the region of very high mass of the $QQ$ pair? Using e.g. a soft $W$, likely radiated by the initial state, to single out the $q\bar{q} \to Q\bar{Q}$ production channel? **Possible study of the charge asymmetry $A_C$ for bottom quarks, as was done for top quarks?**

---

[28]Editors: tbd; contributors: alpgen, sherpa, aMC@NLO, Maltoni/Oleari/Alioli/Reina

| Proc | $WWW$ | $WWZ$ | $WZZ$ | $ZZZ$ |
|------|-------|-------|-------|-------|
| $\sigma$(fb) | $4.3 \times 10^3$ | $4.0 \times 10^3$ | $1.4 \times 10^3$ | $2.6 \times 10^2$ |

| Proc | $WWWW$ | $WWWZ$ | $WWZZ$ | $WZZZ$ | $ZZZZ$ |
|------|--------|--------|--------|--------|--------|
| $\sigma$(fb) | 41 | 60 | 33 | 7.1 | 0.8 |

**Table 3:** NLO cross sections for production of multiple gauge bosons, at 100 TeV [32].

## 11   Production of multiple heavy objects[29]

Most results in this category are already available, see e.g. [32, 34, 35]. Document them in some detail. What is missing is some good motivation for these studies: what can be learned from these multi-body final states? Is there anything unique? For multiple gauge bosons the answer could be in the determination or anomalous higher-order couplings (quartic, quintic, etc). What physics motivation could drive the study of multi-top or associated multi-top/multi-gauge boson production?

### 11.1   Production of multiple gauge bosons

Table 3 shows the rates of associated production of multiple gauge boson [32, 34]. Even including the branching ratios for the best visible leptonic decays, the rates are sufficient in principle to observe the production of up to 4 gauge bosons. This will lead to unprecendeted precision in the measurement of anomalous triple gauge couplings, and to the detection of quartic couplings, furthermore providing a probe of anomalous higher-dimension operators involving multiple gauge bosons.

### 11.2   Multi top-quark production

### 11.3   Multi Higgs boson production by gluon fusion and VBF

### 11.4   Multi Higgs boson production in association with top pairs or gauge bosons

### 11.5   Other rare processes

---

[29]Contributors: aMC@NLO/Sherpa/Torrielli, arXiv:1407.1623

## 12 Loop-induced processes

Valentin/Torrielli. Interesting because of gluon enhancement. Look up Valentin's talk at Loopfest.

# 13 Higgs

The theoretical component of this section will be developed under the responsibility of the SM group, but will end up in the Higgs Chapter of the Report

## 13.1 Higgs production rates

We summarize here, for reference, the production rates at 100 TeV of SM Higgs bosons, including both the canonical production channels, as well as more rare channels of associated production. Associated production of Higgs bosons with other objects could allow independent tests of the Higgs boson properties, and might provide channels with improved signal over background, with possibly reduced sistematic uncertainties.

|  | $gg \rightarrow H$ | $VBF$ | $HW^{\pm}$ | $HZ$ | $t\bar{t}H$ |
|---|---|---|---|---|---|
| $\sigma$(pb) | 740 | 82 | 15.9 | 11.3 | 37.9 |
| $\sigma$(100 TeV)/$\sigma$(14 TeV) | 14.7 | 18.6 | 9.7 | 12.5 | 61 |

**Table 4:** Upper row: cross sections [35] for production of a SM Higgs boson in $gg$ fusion, vector boson fusion, associated production with $W$ and $Z$ bosons, and associated production with a $t\bar{t}$ pair. Lower row: rate increase relative to 14 TeV. All results are NNLO, except $ttH$ (NLO), with the central PDF from the MSTW2008(N)NLO set.

Table 4, extracted from the compilation produced by the LHC Higgs Cross Section working group [35], shows the rates for channels that will already be accessible and used at the LHC. The rates are typically a factor of 10-20 larger than at the LHC, except for the associate $t\bar{t}H$ production, where the $gg$ initial state and the large mass of the final state benefit more significantly from the higher energy, leading to a rate growth by a factor of 60. The samples obtained with a luminosity of 10 ab$^{-1}$ will therefore be a factor of 30-200 larger than what available after the completion of the HL-LHC progamme. The statistical uncertainties for the extraction of the Higgs couplings to the third generation fermions, to the charm and the muon, and to the EW gauge bosons, will become smaller than the percent level. It is difficult today to estimate how the theoretical progress will improve the theoretical systematics, and the determination of experimental systematics will require detailed simulation studies, based on realistic detector concepts. The large statistics for both signals and backgrounds will certainly help in improving the modeling systematics, which in many cases are a limitation to the precision foreseen for the HL-LHC. It is therefore not excluded that the final uncertainties, at least in some channels, may reach the percent level.

An example is the extraction of the top Yukawa coupling $y_{top}$ from the $t\bar{t}H$ process [36]. The large cross section at 100 TeV allows to consider boosted topologies for the hadronic decays of both the top quarks and the Higgs boson ($H \rightarrow b\bar{b}$), placing tight cuts on the emerging jets, and drastically reducing the various sources of backgrounds, while maintaining a statistical sensitivity on the production rate at the percent level. This matches the theoretical systematics, which, already today, is at the percent level [36], if one considers the ratio $\sigma(t\bar{t}H)/\sigma(t\bar{t}Z)$, which is very stable with respect to PDF and scale uncertainties. The branching ratio for the $H \rightarrow b\bar{b}$ decay, needed to extract the top Yukawa coupling from this measurement, will be known with sufficient accuracy if an $e^+e^-$ Higgs factory (at a linear or circular collider) will be operating. Otherwise, a percent-level measurement of $y_{top} * \mathrm{BR}(H \rightarrow b\bar{b})$ will still be one of the most precise determinations of a combination of Higgs couplings, with direct sensitivity on $y_{top}$.

Studies are also available [37–40] of the determination of the Higgs self-coupling in the $HH \rightarrow$

| | $HH$ | $HHjj$ (VBF) | $HHW^{\pm}$ | $HHZ$ | $HHt\bar{t}$ | $HHtj$ |
|---|---|---|---|---|---|---|
| $\sigma$(fb) | $1.2 \cdot 10^3$ | 81 | 8.1 | 5.5 | 86 | 4.6 |

**Table 5:** NLO cross sections for production of a SM Higgs boson pair, including associated production channels, at 100 TeV [34].

| | $HW^+W^-$ | $HW^{\pm}Z$ | $HZZ$ | $HW^{\pm}\gamma$ | $HZ\gamma$ |
|---|---|---|---|---|---|
| $\sigma$(fb) | 170 | 100 | 42 | 78 | 43 |

**Table 6:** NLO cross sections for associated production of a SM Higgs boson with multiple gauge bosons [34].

$b\bar{b}\gamma\gamma$ decay channel[30], with a projected uncertainty on the measurement of the SM coupling in the range of $5-10\%$ with a total of 30 ab$^{-1}$.

Table 5, extracted from the NLO results of Ref. [34], reports the rates for SM Higgs pair production, including channels of associated production with jets, gauge bosons and top quarks. Once again, the possible implications of the measurement and study of these exotic Higgs production channels are under study.

Table 6, extracted from the NLO results of the aMC@NLO code [32, 34], reports the rates for associated production of a SM Higgs with gauge boson pairs. Theoretical systematics, including scale and PDF uncertainties, are typically below 10%.

### 13.2 Inclusive ggF Higgs production
Babis et al for N3LO

### 13.3 Higgs transverse momentum
Grazzini?

### 13.4 Higgs plus jet production
Caola for NNLO

### 13.5 Higgs plus multi-jets
GoSam

### 13.6 Associated Higgs production
### 13.7 VBF Higgs production
Jaeger, Karlberg et al. (for NNLO)

### 13.8 VBF Higgs plus jet production
Jaeger

---

[30]For a study of more rare decay modes, see Ref. [41].

### 13.9 ttH production

Will include discussion of $t\bar{t}H/t\bar{t}Z$, as in arXiv:1507.08169

### 13.10 Higgs constraints from Vector Boson fusion and scattering

Ellis?

### 13.11 Double Higgs production

# 14 Vector Boson fusion gauge boson production[31]

Section to be later included in the Higgs chapter of the report

## 14.1 $Z$ and $W$ production

## 14.2 $ZZ$ and $WW$ production

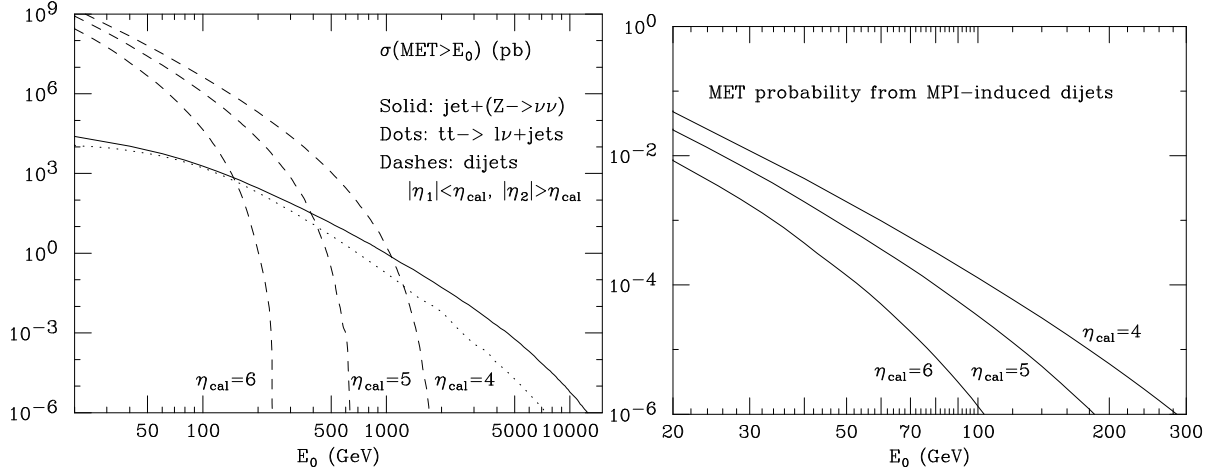## 14.3 Same sign $WW$ production

## 14.4 Anomalous couplings

---

[31]Contributors: Jaeger, ...

## 15   Sources of missing transverse energy[32]



**Fig. 16:** Left: Missing transverse energy rates, from jet+($Z \to \nu\bar{\nu}$) events and from dijets, with a jet escaping undetected at large rapidity. Right: Missing transverse energy probability induced by multiple-parton interactions, for different values of the jet rapidity acceptance.

Missing transverse energy ($\not{E}_T$) is an important signature for many BSM processes. At 100 TeV, SM sources of $\not{E}_T$ can contribute with very large rates of irreducible backgrounds. We consider here, for illustration, the effect of three of the leading sources of irreducible $\not{E}_T$: the associated production of jets and a $Z^0$ boson decaying to neutrinos, the semileptonic decay of top quarks, and the production of jets outside the calorimeter acceptance. The latter channel is important, since the high energy available in the CM allows for the production of large $p_T$ jets at very forward rapidities. This is shown in Fig. 16, where the dashed lines correspond to the rate of dijet events in which one jet is within the calorimeter acceptance (defined by the $\eta_{cal}$ label), and the other is outside. With the standard LHC calorimeter coverage, $\eta_{cal} = 5$, dijets would give a $\not{E}_T$ signal larger than $Z$+jets for $\not{E}_T$ up to $\sim 400$ GeV. This is reduced to $\sim 150$ GeV with a calorimeter extending out to $\eta_{cal} = 6$.

It must be noticed that the limited calorimeter acceptance can induce a $\not{E}_T$ signal in any hard process, due to the finite probability of the coincidence of a multiparton interaction. Multiparton interactions are hard scatterings taking place among the partons not engaged in the primary hard process, and cannot be separated experimentally since the resulting particles emerge from exactly the same vertex as the primary scattering. The probability that a multiparton interaction leads to a secondary hard process $X$ in addition to the primary one is parameterized as $\sigma(X)/\sigma_0$, where $\sigma_0$ is a process-independent parameter. The right plot of Fig. 16 shows the probability of multiparton interactions leading to dijet final states, with one jet inside the calorimeter and the other outside. For this example we chose $\sigma_0 = 30$ mb, a number consistent with the direct experimental determinations from Tevatron and LHC data. $\not{E}_T$ signals in the range of 30-70 GeV are induced with probability of about $10^{-3}$ if $\eta_{cal}$ is in the range 4 to 6, stressing once again the need to instrument the detectors with a calorimetric coverage more extended than at the LHC.

**To be added (among other things):**

– Sources of lepton+$\not{E}_T$: off-shell $W$ production, $W + (Z \to \nu\bar{\nu})$
– Sources of dileptons+$\not{E}_T$: $t\bar{t}$, $off-shell Z \to \ell^+\ell^- + (Z \to \nu\bar{\nu})$, $W^+W^- + (Z \to \nu\bar{\nu})$, etc. Plot e.g. $\not{E}_T$ rates for different values of $M(\ell^+\ell^-)$.

Anything else?

---

[32]Contributors: Jaeger, ...

# 16 SM physics of boosted objects[33]

The ability to tag the nature of the partons that originate the jets at these energies could be crucial to understand the properties of possible signals of new physics, such as a decaying resonance with a multi-TeV mass. Some general features of multi-TeV jets from the QCD background processes, or from the evolution and hadronic decay of bottom, top or $W$ bosons, are shown in Figs. 17-19.
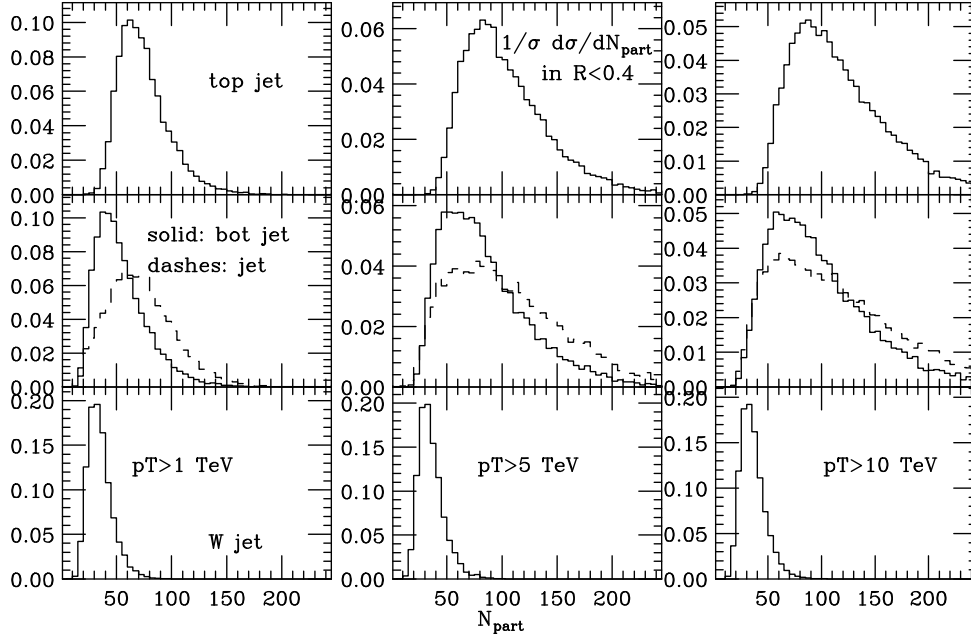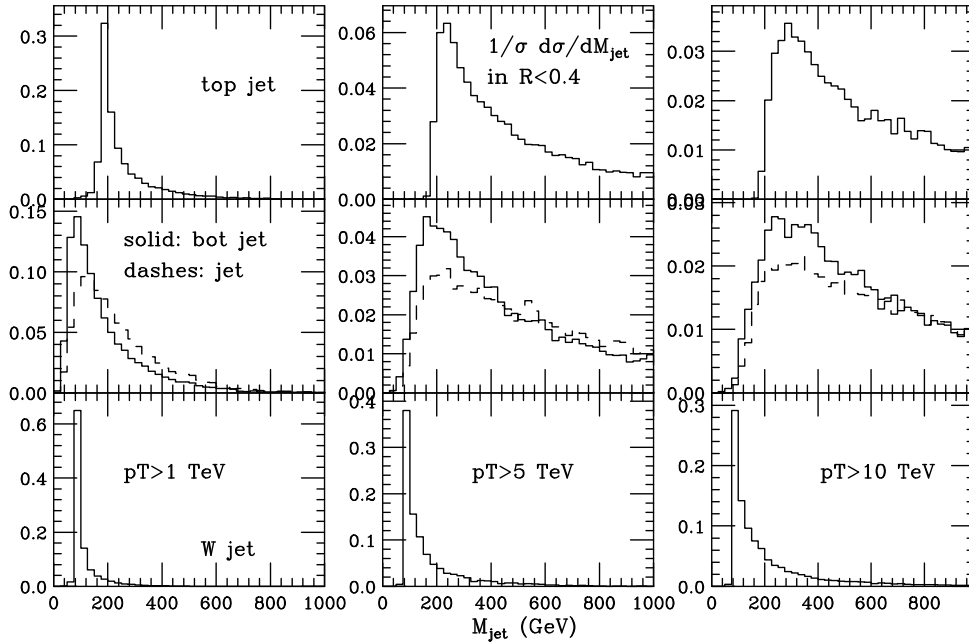


**Fig. 17:** Multiplicity distribution in high-$p_T$ jets orginating from hadronically decaying top quarks (upper rows), bottom quarks and light partons (central rows) and hadronic decays of $W$ bosons (lower rows).
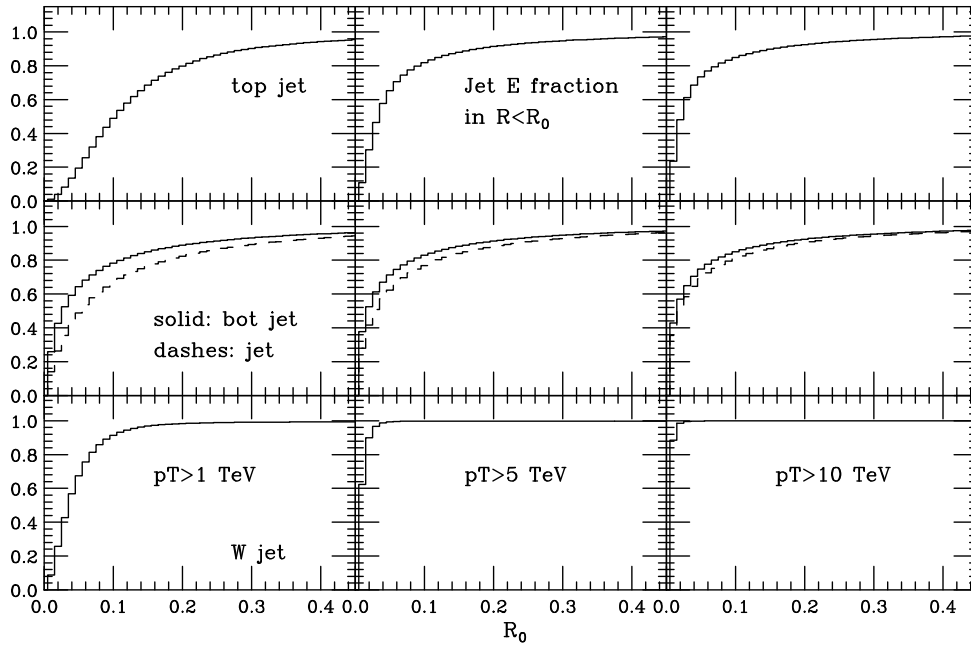


**Fig. 18:** Fraction of the total energy for $R = 1$ jets, contained within smaller radii $R_0$.

---

[33]Editor: A.Larkowski, contributors: Salam, Pierini, Selvaggi, ...

**Fig. 19:** Distribution of the jet invariant mass contained with a cone of radius $R = 0.4$ around the jet axis.

Figure 17 plots the multiplicity distribution of particles (both charged and neutral, assuming stable $\pi^0$'s) contained within a cone of radius $R = 0.4$ around the jet axis. The three columns of plots refer to jets of $p_T > 1$, 5 and 10 TeV, respectively (jets are defined here by the anti-$k_T$ algorithm [42], with a wide cone of $R = 1$). The three rows contain the distributions relative to hadronically-decaying top jets (upper row), bottom jets and inclusive jets (light quarks and gluons, according to the QCD-predicted fraction), and hadronically-decaying $W$ bosons (lower row). For $W$ bosons, the multiplicity is practically independent of $p_T$, and reflects the multiplicity of a $W$ decay at rest, with a negligible contamination from initial-state radiation. The other objects show a clear evolution with $p_T$, and tend asymptotically to very similar spectra, as expected since at large $p_T$ the differences induced by the bottom and top masses, and by the top decay products, are reduced. Notice of course that the multiplicity of top jets has a sharp onset at about $N_{part} \sim 40$, because of the presence of the $W$ decay products. Similar features are observed in the distribution of the jet energy fraction contained in a subcone of radius $R_0$, shown in Fig. 18, and in the distribution of the jet mass within a cone of $R = 0.4$, shown in Fig. 19. Figure 18, in particular, shows that practically all the energy from a 10 TeV $W$ jet is contained within a cone of radius $R \lesssim 0.02$; this means an average of 40 particles all inside this tiny radius, making their individual reconstruction experimentally very challenging. Efforts are ongoing to exploit the small differences observed in distributions such as those shown here, in order to statistically separate with good efficiency objects such as top quarks of gauge bosons from each other, and from lights jets. Such techniques, developed for the $p_T \sim$TeV range of relevance to LHC physics, are being extended to the more challenging multi-TeV regime relevant to the future physics of a 100 TeV collider. See for example the study in Ref. [43], dedicated to top quarks.

# References

[1] R. M. Barnett, H. E. Haber, and D. E. Soper, *Ultraheavy Particle Production from Heavy Partons at Hadron Colliders*, Nucl. Phys. **B306** (1988) 697.

[2] F. I. Olness and W.-K. Tung, *When Is a Heavy Quark Not a Parton? Charged Higgs Production and Heavy Quark Mass Effects in the QCD Based Parton Model*, Nucl. Phys. **B308** (1988) 813.

[3] R. D. Ball et al., *Parton distributions with LHC data*, Nucl. Phys. **B867** (2013) 244–289, `arXiv:1207.1303 [hep-ph]`.

[4] M. A. G. Aivazis, J. C. Collins, F. I. Olness, and W.-K. Tung, *Leptoproduction of heavy quarks. 2. A Unified QCD formulation of charged and neutral current processes from fixed target to collider energies*, Phys. Rev. **D50** (1994) 3102–3118, `arXiv:hep-ph/9312319 [hep-ph]`.

[5] J. C. Collins, *Hard scattering factorization with heavy quarks: A General treatment*, Phys. Rev. **D58** (1998) 094002, `arXiv:hep-ph/9806259 [hep-ph]`.

[6] T. Han, J. Sayre, and S. Westhoff, *Top-Quark Initiated Processes at High-Energy Hadron Colliders*, `arXiv:1411.2588 [hep-ph]`.

[7] A. Denner, S. Dittmaier, T. Kasprzik, and A. Muck, *Electroweak corrections to dilepton + jet production at hadron colliders*, JHEP **06** (2011) 069, `arXiv:1103.0914 [hep-ph]`.

[8] M. Rubin, G. P. Salam, and S. Sapeta, *Giant QCD K-factors beyond NLO*, JHEP **09** (2010) 084, `arXiv:1006.2144 [hep-ph]`.

[9] S. Moretti, M. R. Nolten, and D. A. Ross, *Weak corrections to four-parton processes*, Nucl. Phys. **B759** (2006) 50–82, `arXiv:hep-ph/0606201 [hep-ph]`.

[10] G. Bell, J. H. Kuhn, and J. Rittinger, *Electroweak Sudakov Logarithms and Real Gauge-Boson Radiation in the TeV Region*, Eur. Phys. J. **C70** (2010) 659–671, `arXiv:1004.4117 [hep-ph]`.

[11] S. Dittmaier, A. Huss, and C. Speckner, *Weak radiative corrections to dijet production at hadron colliders*, JHEP **11** (2012) 095, `arXiv:1210.0438 [hep-ph]`.

[12] J. R. Christiansen and T. Sjostrand, *Weak Gauge Boson Radiation in Parton Showers*, JHEP **04** (2014) 115, `arXiv:1401.5238 [hep-ph]`.

[13] A. Hook and A. Katz, *Unbroken SU(2) at a 100 TeV collider*, JHEP **09** (2014) 175, `arXiv:1407.2607 [hep-ph]`.

[14] B. W. Lee, C. Quigg, and H. B. Thacker, *Weak Interactions at Very High-Energies: The Role of the Higgs Boson Mass*, Phys. Rev. **D16** (1977) 1519.

[15] M. S. Chanowitz and M. K. Gaillard, *The TeV Physics of Strongly Interacting W's and Z's*, Nucl. Phys. **B261** (1985) 379.

[16] G. L. Kane, W. W. Repko, and W. B. Rolnick, *The Effective W+-, Z0 Approximation for High-Energy Collisions*, Phys. Lett. **B148** (1984) 367–372.

[17] S. Dawson, *The Effective W Approximation*, Nucl. Phys. **B249** (1985) 42–60.

[18] J. Chen, T. Han, R. Ruiz, and B. Tweedie. In preparation.

[19] M. Cvetic and P. Langacker, *Rare decays as diagnostics for Z-prime gauge couplings at hadron colliders*, Phys. Rev. **D46** (1992) R14–R18.

[20] T. G. Rizzo, *Exploring new gauge bosons at a 100 TeV collider*, Phys. Rev. **D89** (2014) no. 9, 095022, `arXiv:1403.5465 [hep-ph]`.

[21] J. Alwall, M. Herquet, F. Maltoni, O. Mattelaer, and T. Stelzer, *MadGraph 5 : Going Beyond*, JHEP **06** (2011) 128, `arXiv:1106.0522 [hep-ph]`.

[22] T. Stelzer and W. F. Long, *Automatic generation of tree level helicity amplitudes*, Comput. Phys. Commun. **81** (1994) 357–371, `arXiv:hep-ph/9401258 [hep-ph]`.

[23] F. Maltoni and T. Stelzer, *MadEvent: Automatic event generation with MadGraph*, JHEP **02** (2003) 027, `arXiv:hep-ph/0208156 [hep-ph]`.

[24] S. Dimopoulos and G. Giudice, *Naturalness constraints in supersymmetric theories with nonuniversal soft terms*, Phys.Lett. **B357** (1995) 573–578, `arXiv:hep-ph/9507282 [hep-ph]`.

[25] A. G. Cohen, D. B. Kaplan, and A. E. Nelson, *The More minimal supersymmetric standard model*, Phys. Lett. **B388** (1996) 588–598, `arXiv:hep-ph/9607394 [hep-ph]`.

[26] C. Brust, A. Katz, S. Lawrence, and R. Sundrum, *SUSY, the Third Generation and the LHC*, JHEP **03** (2012) 103, `arXiv:1110.6670 [hep-ph]`.

[27] R. Essig, E. Izaguirre, J. Kaplan, and J. G. Wacker, *Heavy Flavor Simplified Models at the LHC*, JHEP **01** (2012) 074, `arXiv:1110.6443 [hep-ph]`.

[28] M. Papucci, J. T. Ruderman, and A. Weiler, *Natural SUSY Endures*, JHEP **09** (2012) 035, `arXiv:1110.6926 [hep-ph]`.

[29] M. Mangano and T. Melia, *Rare exclusive hadronic W decays in a $t\bar{t}$ environment*, Eur. Phys. J. **C75** (2015) no. 6, 258, `arXiv:1410.7475 [hep-ph]`.

[30] O. Gedalia, G. Isidori, F. Maltoni, G. Perez, M. Selvaggi, et al., *Top B Physics at the LHC*, Phys.Rev.Lett. **110** (2013) no. 23, 232002, `arXiv:1212.4611 [hep-ph]`.

[31] F. Maltoni, M. L. Mangano, I. Tsinikos, and M. Zaro, *Top-quark charge asymmetry and polarization in $t\bar{t}W^{\pm}$ production at the LHC*, Phys. Lett. **B736** (2014) 252–260, `arXiv:1406.3262 [hep-ph]`.

[32] P. Torrielli, *Rare Standard Model processes for present and future hadronic colliders*, `arXiv:1407.1623 [hep-ph]`.

[33] F. Maltoni, D. Pagani, and I. Tsinikos, *Associated production of a top-quark pair with vector bosons at NLO in QCD: impact on $t\bar{t}H$ searches at the LHC*, `arXiv:1507.05640 [hep-ph]`.

[34] J. Alwall, R. Frederix, S. Frixione, V. Hirschi, F. Maltoni, et al., *The automated computation of tree-level and next-to-leading order differential cross sections, and their matching to parton shower simulations*, JHEP **1407** (2014) 079, `arXiv:1405.0301 [hep-ph]`.

[35] *Higgs Cross Section Working Group*, `https://cern.ch/twiki/bin/view/LHCPhysics/LHCHXSWG`.

[36] M. Mangano, T. Plehn, P. Reimitz, T. Schell, and H.-S. Shao, *Measuring the Top Yukawa Coupling at 100 TeV*, `arXiv:1507.08169 [hep-ph]`.

[37] W. Yao, *Studies of measuring Higgs self-coupling with $HH \to b\bar{b}\gamma\gamma$ at the future hadron colliders*, `arXiv:1308.6302 [hep-ph]`.

[38] H.-J. He, J. Ren, and W. Yao, *Probing New Physics of Cubic Higgs Interaction via Higgs Pair Production at Hadron Colliders*, `arXiv:1506.03302 [hep-ph]`.

[39] A. J. Barr, M. J. Dolan, C. Englert, D. E. F. de Lima, and M. Spannowsky, *Higgs Self-Coupling Measurements at a 100 TeV Hadron Collider*, `arXiv:1412.7154 [hep-ph]`.

[40] A. Azatov, R. Contino, G. Panico, and M. Son, *Effective field theory analysis of double Higgs production via gluon fusion*, `arXiv:1502.00539 [hep-ph]`.

[41] A. Papaefstathiou, *Discovering Higgs boson pair production through rare final states at a 100 TeV collider*, Phys. Rev. **D91** (2015) no. 11, 113016, `arXiv:1504.04621 [hep-ph]`.

[42] M. Cacciari, G. P. Salam, and G. Soyez, *The Anti-k(t) jet clustering algorithm*, JHEP **04** (2008) 063, `arXiv:0802.1189 [hep-ph]`.

[43] A. J. Larkoski, F. Maltoni, and M. Selvaggi, *Tracking down hyper-boosted top quarks*, JHEP **06** (2015) 032, `arXiv:1503.03347 [hep-ph]`.